

FedSCS-XGB - Federated Server-centric surrogate XGBoost for continual health monitoring

Felix Walger

Chair of Information Theory and Data Analytics (INDA)
RWTH Aachen University
Aachen, Germany
felix.walger@inda.rwth-aachen.de

Mehdi Ejtehad

Spinal Cord Injury Artificial Intelligence (SCAI) Lab
ETH Zürich & Swiss Paraplegic Research (SPF)
Nottwil, Switzerland
mehdi.ejtehad@hest.ethz.ch

Anke Schmeink

Chair of Information Theory and Data Analytics (INDA)
RWTH Aachen University
Aachen, Germany
anke.schmeink@inda.rwth-aachen.de

Diego Paez-Granados

Spinal Cord Injury Artificial Intelligence (SCAI) Lab
ETH Zürich & Swiss Paraplegic Research (SPF)
Nottwil, Switzerland
diego.paez@hest.ethz.ch

Abstract—Wearable sensors with local data processing can detect health threats early, enhance documentation, and support personalized therapy. In the context of spinal cord injury (SCI), which involves risks such as pressure injuries and blood pressure instability, continuous monitoring can help mitigate these by enabling early detection and intervention. In this work, we present a novel distributed machine learning (DML) protocol for human activity recognition (HAR) from wearable sensor data based on gradient-boosted decision trees (XGBoost). The proposed architecture is inspired by Party-Adaptive XGBoost (PAX) while explicitly preserving key structural and optimization properties of standard XGBoost, including histogram-based split construction and tree-ensemble dynamics. First, we provide a theoretical analysis showing that, under appropriate data conditions and suitable hyperparameter selection, the proposed distributed protocol can converge to solutions equivalent to centralized XGBoost training. Second, the protocol is empirically evaluated on a representative wearable-sensor HAR dataset, reflecting the heterogeneity and data fragmentation typical of remote monitoring scenarios. Benchmarking against centralized XGBoost and IBM PAX demonstrates that the theoretical convergence properties are reflected in practice. The results indicate that the proposed approach can match centralized performance up to a gap under 1% while retaining the structural advantages of XGBoost in distributed wearable-based HAR settings.

Index Terms—Distributed machine learning, Federated learning, XGBoost, Gradient-boosted decision trees, Human activity recognition, Wearable sensors, Biomedical signal processing, Privacy-preserving learning

I. INTRODUCTION

Many chronic health conditions face a lifelong and evolving risk of Secondary Health Conditions (SHCs). Individuals with Spinal Cord Injury (SCI) live with chronic pain, pressure injuries, and cardiometabolic complications, which frequently intensify after discharge into community living [1], [2]. These risks exhibit pronounced inter-individual variability and long-term temporal dynamics driven by injury characteristics, aging, and everyday behavior, rendering episodic clinical assessment insufficient. Wearable sensing enables continuous observation

of functional and physiological patterns in daily life, but resulting data streams are inherently heterogeneous, non-stationary, and privacy-sensitive. Human Activity Recognition (HAR) models trained on such data implicitly encode sensitive behavioral and health-related information [3], [4], which cannot be reliably disentangled once transmitted to a central entity [5]. Distributed Machine Learning (DML) addresses this challenge by enabling collaborative model training while retaining raw sensor data locally, thereby supporting personalization under non-IID data and limiting information leakage [6], [7]. Gradient-boosted decision trees such as XGBoost [8] provide deterministic inference, predictable computational complexity, and interpretable decision logic through tree splits and additive structure [9], [10]. These properties make them attractive for edge-based biomedical HAR, but standard XGBoost training assumes centralized access to the full dataset, which conflicts with privacy-preserving wearable deployments. To bridge this gap, we propose a foundational DML protocol for XGBoost-based wearable monitoring for chronic lifelong conditions such as SCI, conceptually shown in Fig. 1. The protocol enables distributed, privacy-aware training while preserving the key mathematical and optimization behavior of centralized, histogram-based boosting. Inspired by existing work [11], our approach places stronger emphasis on retaining native histogram construction and split-finding dynamics, rather than adapting model structure to protocol constraints.

The main contributions of this work are:

- 1) an analysis of fundamental requirements for distributed machine learning in lifelong monitoring - focused on chronic health conditions,
- 2) design of a PAX-inspired distributed XGBoost protocol, preserving core boosting and histogram mechanisms,
- 3) a convergence analysis demonstrating equivalence to centralized XGBoost under suitable conditions, and
- 4) an evaluation on feature-extracted HAR data based on a

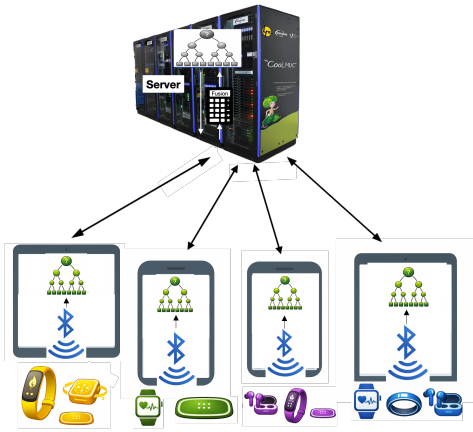


Fig. 1. A continual health monitoring system with FL.

emulated implementation using Flower [12].

II. RELATED WORK

FL is a central paradigm for privacy-preserving model training across distributed wearable and mobile sensors and has been widely adopted for HAR. By enabling collaborative learning without centralizing raw sensor data, FL directly addresses privacy and data governance concerns [13]. Early feasibility studies [14] showed that baseline algorithms such as *FedAvg* can achieve competitive performance relative to centralized training, while also revealing sensitivity to client heterogeneity and data imbalance. Subsequent work therefore introduced architectural extensions to improve robustness and scalability, including hierarchical FL [15], hybrid horizontal-vertical federation [16], and cluster-based aggregation strategies [17].

Personalization has emerged as a dominant research direction in FL-based HAR. Approaches such as *FedHealth* [18], *Proto-HAR* [19], and meta-learning-based methods [20] explicitly separate shared representations from user-specific adaptation, consistently outperforming purely global models under heterogeneous client distributions.

Recent studies address deployment-related constraints on heterogeneous edge devices. Adaptive systems such as *Hydra* [21] and knowledge-distillation-based FL methods [22] reduce communication and computation overhead. Complementary system-level analyses [23] investigate robustness under bandwidth limitations and asynchronous updates, while additional work focuses on privacy compliance through encryption and machine unlearning mechanisms [24]. However, Most existing FL research in HAR focuses on neural network architectures, while federated ensemble methods remain comparatively underexplored. For horizontal FL settings several Federated XGBoost approaches have been proposed.

A foundational contribution is *Party-Adaptive XGBoost* (PAX) [11], which extends XGBoost’s histogram-based split finding using client-specific quantile sketches. These sketches are aggregated at the server to construct globally consistent split candidates without exposing raw data. Subsequent stud-

ies [25] demonstrate that Federated XGBoost maintains performance close to centralized training even under severe sample-wise non-IID partitions, highlighting the inherent robustness of tree-based models.

To further reduce communication overhead, [26] propose a gradient-less Federated XGBoost approach that aggregates locally trained ensembles instead of gradients or histograms. Alternative work explores improved sampling strategies, such as Minimal Variance Sampling [27], to enhance split quality under limited communication. A recent survey [28] categorizes these methods into histogram-based, ensemble-aggregation, and sampling-enhanced approaches, outlining their respective trade-offs. Despite substantial progress, current distributed learning approaches for HAR exhibit several limitations. Many frameworks are highly scenario-specific and rely on deep neural networks that are computationally demanding for long-term edge deployment [20]. Moreover, ensemble-based methods such as XGBoost remain underrepresented in federated HAR, despite their advantages in interpretability, energy efficiency, and robustness to heterogeneous data. Motivated by these gaps, this work investigates a communication-efficient and privacy-preserving Federated XGBoost framework tailored to heterogeneous wearable sensor data, with a focus on scalable and interpretable activity recognition in real-world rehabilitation scenarios.

III. METHODS

A. Sensory System, ADLs, and Data Processing

Based on the prior validated ADL recognition framework in [3], we consider **16** clinically relevant ADLs/states for classification using the unobtrusive multimodal sensor configuration in Fig. 2, covering wheelchair activities (resting, phone/computer use, arm raises, eating/drinking, hand cycling), mobility modes (assisted/self propulsion), transfer events (to/from wheelchair), pressure relief, four lying postures (back/right/left/stomach), and the empty-wheelchair state.

The time series data were processed using a 5th-order Butterworth low-pass filter with a cut-off frequency of 5 Hz (10 Hz for the wheel IMU) [3]. The filtered signals were resampled to 20 Hz to reduce computational complexity and segmented using a sliding-window approach; based on preliminary experiments, a 4 s window with a 2 s step (50% overlap) was used. Overall, data from 8 individuals were included, yielding 44,358 windows across the 16 classes, with moderate class imbalance: phone/computer/eating typically contributed $\sim 600\text{--}700$ windows per subject, posture and propulsion-related classes were commonly around ~ 300 windows per subject, and transfer activities were comparatively sparse (tens to a few hundred windows per subject).

For feature extraction, we used the TIFEX-Py toolbox [29] to compute a compact set of time- and frequency-domain descriptors per window, including first- and second-order statistics (mean, standard deviation, variance, median, min/max), higher-order moments (skewness, kurtosis), change/complexity measures (absolute sum of changes, mean change, mean absolute change, longest strike above/below

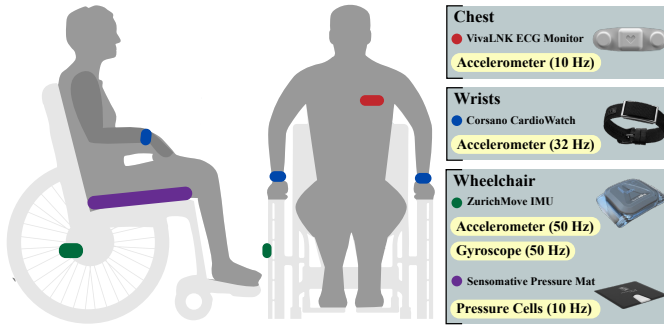


Fig. 2. Sensor setup for the SCI wheelchair user: VivaLNK Wearable ECG monitor sensor on chest, two Corsano’s CardioWatch 287-2 worn at wrists, Sensomative wheelchair mat placed under bottom cushion, and Zurichmove IMU on the wheel of the wheelchair.

mean, sample entropy, CID-CE), and spectral/periodicity features (FFT coefficient magnitude, Welch density, autocorrelation, number of peaks, and zero-crossing rate).

B. FedSCS-XGB

We introduce here a PAX-inspired Federated implementation of XGBoost called Federated Server-Centric Surrogate XGBoost.

a) Protocol overview: FedSCS-XGB alternates two phases. In sketch rounds, clients transmit mergeable per-feature DDSketches weighted by (diagonal) Hessians; the server merges these sketches and derives global bin edges. In atom rounds, clients quantize samples using the received edges, aggregate sufficient statistics (W, G, H) per multi-feature bin vector (atom key), and transmit these atom summaries. The server conditions atoms on the current node-path, evaluates histogram split candidates, selects the best split per node, and returns the resulting stump(s) to clients to update local margins. The protocol procedures are illustrated in Algorithms 2 and 1.

b) Multiclass softmax and tree groups.: For multiclass classification with K classes, the client computes softmax probabilities and per-class gradients/Hessians. The server grows one tree per class per boosting round (XGBoost *tree group* semantics), i.e., it evaluates gains per class and sums them to select splits; leaf weights are class-wise vectors.

c) Relation to PAX: Fed SCS-XGB is inspired by the Party-Adaptive XGBoost (PAX) framework of Ong *et al* [30], but differs in several key aspects. While PAX constructs party-specific surrogate *feature representations* and associated histogram statistics to guide split evaluation, Fed SCS-XGB explicitly separates bin-edge estimation and sufficient-statistic aggregation into two synchronous communication phases. In particular, global bin edges are determined via Hessian-weighted, mergeable sketches, after which clients transmit only aggregated atom statistics per multi-feature bin vector. Furthermore, Fed SCS-XGB performs local prediction and gradient computation on raw feature values and uses the surrogate bins solely for aggregation, whereas PAX conceptually evaluates split candidates with respect to the surrogate feature

Algorithm 1 FedSCS-XGB Server (multiclass: Sketch \rightarrow Atoms)

Require: Rounds T , features d , bins B , depth D , reg. λ, γ

- 1: Initialize global additive model $f^{(A)} \leftarrow 0$
- 2: **for** $t = 1, \dots, T$ **do**
- 3: Sample clients C_t
- 4: **Phase 1 (Sketch).** \triangleright **Comm:** $S \rightarrow C$
- 5: Send SKETCH_REQ(t, B) to all $c \in C_t$
- 6: **Barrier:** await $\{\mathcal{K}_{c,f}^{(t)}\}_{f=1}^d$ from all $c \in C_t$
- 7: **for** $f = 1, \dots, d$ **do**
- 8: $\mathcal{E}_f^{(t)} \leftarrow \text{QUANTILES}(\text{MERGE}(\{\mathcal{K}_{c,f}^{(t)}\}_{c \in C_t}), B)$
- 9: **end for**
- 10: **Phase 2 (Atoms).** \triangleright **Comm:** $S \rightarrow C$
- 11: Send ATOM_REQ($t, f_{t-1}^{(A)}, \mathcal{E}^{(t)}$) to all $c \in C_t$
- 12: **Barrier:** await atom maps $\{(W_r^{(c)}, G_r^{(c)}, H_r^{(c)})\}_{r \in \mathcal{R}_c}$ from all $c \in C_t$
- 13: Merge atoms by key: $(W_r, G_r, H_r) \leftarrow \sum_{c \in C_t} (W_r^{(c)}, G_r^{(c)}, H_r^{(c)})$
- 14: Grow trees depth-wise up to D using histogram split search on atoms:
- 15: **for** each active node a **do**
- 16: **for** each (f, q) with $q \in \{1, \dots, B-1\}$ **do**
- 17: $(G_{L,\cdot}, H_{L,\cdot}, G_{R,\cdot}, H_{R,\cdot}) \leftarrow \text{PREFIXSTATS}(a, f, q; \{(W_r, G_r, H_r)\})$
- 18: Gain(a, f, q) $\leftarrow \sum_{k=1}^K \text{Gain}(G_{L,k}, H_{L,k}, G_{R,k}, H_{R,k})$ using Eq. (1)
- 19: **end for**
- 20: $(f^*, q^*) \leftarrow \arg \max_{f,q} \text{Gain}(a, f, q)$ \triangleright
- 21: deterministic tie-break
- 22: $w_{L,k} \leftarrow -G_{L,k}/(H_{L,k} + \lambda)$, $w_{R,k} \leftarrow -G_{R,k}/(H_{R,k} + \lambda)$
- 23: Add split $(f^*, \theta = \mathcal{E}_{f^*}^{(t)}[q^*], w_L, w_R)$ to $\{T_{t,k}\}_{k=1}^K$
- 24: **end for**
- 25: $f_t^{(A)} \leftarrow f_{t-1}^{(A)} + \eta \cdot \{T_{t,k}\}_{k=1}^K$
- 26: **end for**

representation. These modifications preserve the underlying XGBoost objective while improving communication efficiency and simplifying synchronization, and they form the basis for the convergence analysis presented in this work.

C. Convergence to the Centralized Histogram XGBoost Objective via Hessian-Weighted DDSketch Binning (SCS-XGB)

a) Notation: Table I summarizes all quantities used throughout this subsection.

b) Second-order gain (XGBoost): For a candidate split of a node into left/right parts with sufficient statistics (G_L, H_L) and (G_R, H_R) , the XGBoost gain is

$$\text{Gain}(G_L, H_L, G_R, H_R) := \frac{1}{2} \left(\frac{G_L^2}{H_L + \lambda} + \frac{G_R^2}{H_R + \lambda} - \frac{(G_L + G_R)^2}{(H_L + H_R) + \lambda} \right) - \gamma. \quad (1)$$

Algorithm 2 FedSCS-XGB Client p_i (multiclass softmax)**Require:** Local data (X, y) , N_i samples, K classes, d features

```

1: Maintain margins  $\mathbf{m} \in \mathbb{R}^{N_i \times K}$  (init. 0)
2: while requests arrive do
3:   Receive message from server
4:   if SKETCH_REQ( $t, B$ ) then
5:     Compute per-sample  $(g_{i,k}^{(t)}, h_{i,k}^{(t)})$  (softmax, diag.
Hessian) and weights  $w_i^{(t)} \leftarrow \sum_{k=1}^K h_{i,k}^{(t)}$ 
6:     for  $f = 1, \dots, d$  do
7:       Build weighted sketch  $\mathcal{K}_{i,f}^{(t)}$  from
 $\{(x_{i,f}, w_i^{(t)})\}_{i=1}^{N_i}$ 
8:     end for
9:     Send  $\{\mathcal{K}_{i,f}^{(t)}\}_{f=1}^d$ 
10:    else if ATOM_REQ( $t, f_{t-1}^{(A)}, \mathcal{E}^{(t)}$ ) then
11:      Update margins:  $\mathbf{m} \leftarrow \mathbf{m} + \eta \cdot f_{t-1}^{(A)}(X)$ 
12:      Compute per-sample  $(g_{i,\cdot}^{(t)}, h_{i,\cdot}^{(t)})$  as above
13:      Bin-ID vectors:  $\mathbf{b}_i \leftarrow (\text{BININDEX}(\mathcal{E}_f^{(t)}, x_{i,f}))_{f=1}^d$ 
14:      Aggregate atoms per occupied key  $r$ :
 $(W_r, G_{r,\cdot}^{(t)}, H_{r,\cdot}^{(t)}) \leftarrow \sum_{i:\mathbf{b}_i=r} (1, g_{i,\cdot}^{(t)}, h_{i,\cdot}^{(t)})$ 
15:      Send  $\{(W_r, G_{r,\cdot}^{(t)}, H_{r,\cdot}^{(t)})\}_{r \in \mathcal{R}_i}$ 
16:    end if
17: end while

```

TABLE I
NOTATION FOR THE SCS-XGB CONVERGENCE ANALYSIS.

Symbol	Meaning
$\mathcal{D} = \{(x_j, y_j)\}_{j=1}^N$	Dataset, N samples
$x_j \in \mathbb{R}^d$	Feature vector, d features
M_t	Model after t boosting rounds
T, m	# rounds, max. tree depth
$\ell(y, \hat{y})$	Loss, convex and C^2 in \hat{y}
$g_j^{(t)}, h_j^{(t)}$	First/second derivatives of ℓ
λ, γ	Regularization, split penalty
B	Bins per feature
$f \in \{1, \dots, d\}$	Feature index
$F_f^{(t)}$	Hessian-weighted empirical CDF
$E_f^{(t)}, \tilde{E}_f^{(t)}$	Ideal / sketch histogram edges
α	CDF (rank) approximation error
$\mathbf{b}(x)$	Bin-ID vector induced by $\tilde{E}^{(t)}$
r	Atom (bin-ID) key
$W_r, G_r^{(t)}, H_r^{(t)}$	Atom count, gradient, Hessian
$(G_L, H_L), (G_R, H_R)$	Split sufficient statistics
\mathcal{A}_t	Nodes evaluated at round t
Gain	Split gain (Eq. (1))
$J_t^{\text{cent}}, J_t^{\text{scs}}$	Centralized / SCS-XGB objective

c) *Hessian-weighted quantiles.*: At round t , define the Hessian-weighted empirical CDF for feature f as

$$F_f^{(t)}(v) := \frac{1}{\sum_{j=1}^N h_j^{(t)}} \sum_{j: x_j^{(f)} \leq v} h_j^{(t)}. \quad (2)$$

We define ideal histogram edges by the left-quantile convention

$$e_{f,b}^{(t)} := \inf \left\{ v : F_f^{(t)}(v) \geq b/B \right\}, \quad b = 0, \dots, B. \quad (3)$$

SCS-XGB uses mergeable Hessian-weighted DDSketches to obtain approximate edges $\tilde{E}_f^{(t)} = (\tilde{e}_{f,0}^{(t)} < \dots < \tilde{e}_{f,B}^{(t)})$ [31]; edges are fixed during split search.

d) *Goal.*: For any finite horizon T and tolerance $\varepsilon > 0$, we show existence of a sketch accuracy level $\bar{\alpha}$ such that $\alpha \leq \bar{\alpha}$ implies $|J_t^{\text{scs}} - J_t^{\text{cent}}| \leq \varepsilon$ for all $t \leq T$.

e) *Assumptions.*: **A1 (Bounded derivatives).** $\exists G_{\max}, H_{\max} < \infty$ such that $|g_j^{(t)}| \leq G_{\max}$ and $0 \leq h_j^{(t)} \leq H_{\max}$ for all j, t .

A2 (Bracketing accuracy). $\exists \alpha \in (0, 1)$ such that for all t, f, b ,

$$F_f^{(t)}(\tilde{e}_{f,b}^{(t)} -) \leq \frac{b}{B} + \alpha, \quad F_f^{(t)}(\tilde{e}_{f,b}^{(t)}) \geq \frac{b}{B} - \alpha.$$

A3 (Fixed edges). Within each round t , the edges $\tilde{E}^{(t)}$ are fixed during depth-wise split evaluation. **A4 (Deterministic tie-breaking).** Centralized histogram XGBoost and SCS-XGB break equal-gain ties identically.

Lemma 1 (Exact surrogate equivalence). *Fix a boosting round t and sketch edges $\tilde{E}^{(t)}$. Greedy split evaluation using routed atom statistics is exactly equivalent to running histogram XGBoost on the induced atom pseudo-dataset with edges $\tilde{E}^{(t)}$.*

Proof. Fix t and $\tilde{E}^{(t)}$. For any node and candidate split (f, k) , routing depends only on bin indices and is therefore deterministic. Aggregating $(G_r^{(t)}, H_r^{(t)}, W_r)$ over atom keys yields exactly the left/right sufficient statistics that histogram XGBoost computes on the pseudo-dataset with the same edges. Since the gain (1) depends only on these statistics, all candidate gains and the greedy split selection coincide. \square

Lemma 2 (Hessian prefix-mass perturbation). *Hold A1–A2. Fix t and feature f . Define the ideal and sketch-induced Hessian prefix masses*

$$H_{\leq b}^{(t)} := \sum_{j: x_j^{(f)} \leq e_{f,b}^{(t)}} h_j^{(t)}, \quad \tilde{H}_{\leq b}^{(t)} := \sum_{j: x_j^{(f)} \leq \tilde{e}_{f,b}^{(t)}} h_j^{(t)}.$$

Then, for all $b \in \{0, \dots, B\}$,

$$|\tilde{H}_{\leq b}^{(t)} - H_{\leq b}^{(t)}| \leq \alpha \sum_{j=1}^N h_j^{(t)}.$$

Proof. By Definition (2),

$$\tilde{H}_{\leq b}^{(t)} = \left(\sum_j h_j^{(t)} \right) F_f^{(t)}(\tilde{e}_{f,b}^{(t)}), \quad H_{\leq b}^{(t)} = \left(\sum_j h_j^{(t)} \right) F_f^{(t)}(e_{f,b}^{(t)}).$$

Under the left-quantile convention (3), $F_f^{(t)}(e_{f,b}^{(t)}) \geq b/B$ and $F_f^{(t)}(e_{f,b}^{(t)} -) < b/B$. Combining this with the bracketing condition A2 yields

$$|F_f^{(t)}(\tilde{e}_{f,b}^{(t)}) - F_f^{(t)}(e_{f,b}^{(t)})| \leq \alpha,$$

and multiplying by $\sum_j h_j^{(t)}$ gives the stated bound. \square

f) *Definition (Node-wise statistic perturbation constant):*

Fix a boosting round t and node a . Let $\mathbf{s}_{t,a}(f, k)$ and $\tilde{\mathbf{s}}_{t,a}(f, k)$ denote the ideal and sketch-induced sufficient statistics for candidate split (f, k) . Define $K_{t,a} \geq 0$ such that

$$\sup_{(f,k)} \|\tilde{\mathbf{s}}_{t,a}(f, k) - \mathbf{s}_{t,a}(f, k)\|_1 \leq K_{t,a} \alpha. \quad (4)$$

Such a finite constant exists for fixed data, t , and a whenever statistic perturbations scale linearly in α for sufficiently small α .

Lemma 3 (Lipschitz continuity of the gain). *Fix $\lambda > 0$. The gain functional (1) is Lipschitz continuous on any bounded domain $|G| \leq \bar{G}$, $0 \leq H \leq \bar{H}$, with*

$$|\text{Gain}(\mathbf{s}) - \text{Gain}(\mathbf{s}')| \leq L(\bar{G}, \bar{H}, \lambda) \|\mathbf{s} - \mathbf{s}'\|_1.$$

Proof. On the bounded domain, all denominators are bounded below by $\lambda > 0$, hence all partial derivatives are bounded. The result follows from the mean value theorem. \square

g) *Definition (Node-wise gain sensitivity):* For each (t, a) define

$$C_{t,a} := L(\bar{G}_{t,a}, \bar{H}_{t,a}, \lambda) K_{t,a},$$

where $\bar{G}_{t,a}$ and $\bar{H}_{t,a}$ bound all candidate split statistics at node a .

Lemma 4 (Uniform gain perturbation). *For all candidate splits (f, k) at node a ,*

$$|\text{Gain}(\tilde{\mathbf{s}}_{t,a}(f, k)) - \text{Gain}(\mathbf{s}_{t,a}(f, k))| \leq C_{t,a} \alpha.$$

Theorem 5 (Finite-horizon ε -approximation). *Hold A1–A4. For any $\varepsilon > 0$ and finite horizon T , there exists $\bar{\alpha} > 0$ such that for all $\alpha \leq \bar{\alpha}$ and all $t \leq T$,*

$$|J_t^{\text{scs}} - J_t^{\text{cent}}| \leq \varepsilon.$$

Proof. For node a at round t , uniform gain perturbation implies ideal gain suboptimality at most $2C_{t,a}\alpha$. Since each split reduces the objective by exactly its gain, summing over nodes yields

$$|J_t^{\text{scs}} - J_t^{\text{cent}}| \leq \sum_{a \in \mathcal{A}_t} 2C_{t,a}\alpha =: C_t \alpha.$$

With $C := \max_{t \leq T} C_t < \infty$, choosing $\bar{\alpha} = \varepsilon/C$ proves the claim. \square

h) *Interpretation:* Assumption A2 can be satisfied for arbitrarily small α by choosing sufficiently accurate DDSketch hyperparameters. Thus, for any fixed finite horizon T , SCS-XGB converges to the centralized histogram XGBoost solution in objective value as $\alpha \rightarrow 0$, independently of the underlying data distribution.

A. Implementation

To obtain a realistic and functionally faithful emulation of a deployable Distributed Machine Learning (DML) system, we implemented *FedSCS-XGB* on top of the Flower federated learning framework [12] in Python. We rely on Flower’s standard `server_app / client_app` architecture together with its built-in simulation capabilities, which enable controlled experimentation under reproducible client participation and communication patterns.

As a centralized baseline, we use the reference Python implementation of XGBoost [8]. In addition, we implemented the Party-Adaptive XGBoost (PAX) protocol according to the pseudo-algorithm and design principles described in the original work [30], again using Flower as the orchestration layer.

A key advantage of Flower is its high degree of modularity. This allowed us to clearly separate (i) the distributed machine learning logic, (ii) the data processing pipeline, (iii) the protocol-level communication, control, and orchestration mechanisms, and (iv) the simulation environment. As a result, the implementation remains close to a real world deployment setting while enabling systematic comparison of different distributed learning protocols under identical experimental conditions.

B. Experiments

We trained XGBoost models for 10 boosting rounds to study the effect of histogram bin resolution on performance. Four bin sizes were evaluated: $B \in \{64, 128, 256, 512\}$. Data were split into 80% training and 20% validation sets using a deterministic hash-based partitioning scheme. Pre-processing consisted of feature extraction followed by window mixing to avoid overfitting to temporally correlated segments and to preserve training heterogeneity. Models were trained with a maximum tree depth of 4 and hyperparameters $\lambda = 1.0$, $\gamma = 0.1$, and learning rate $\eta = 0.2$. All 16 classes were used, with the standard XGBoost multiclass softmax loss.

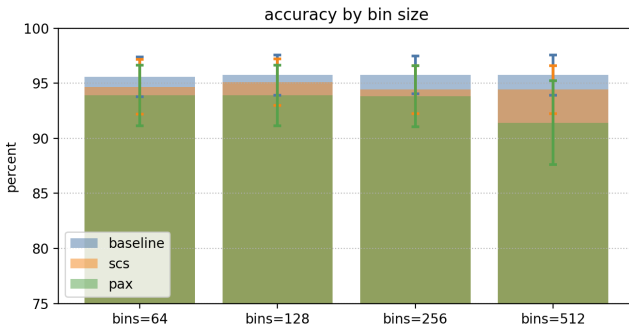
Across all evaluated metrics, FedSCS-XGB closely matches centralized XGBoost and consistently outperforms PAX under identical hyperparameter settings (Fig. 4, 3, Table II). The accuracy gap to the centralized baseline remains below 1.5% point for all bin counts, while PAX exhibits a substantially larger degradation. FedSCS-XGB additionally shows higher and more stable F1-scores across clients, which can be seen in Fig. 3. This is indicating improved robustness under class imbalance and client heterogeneity. Performance remains stable when varying the number of bins from 128 to 512, suggesting limited sensitivity to bin resolution once global alignment is achieved. Conversely, an increase in bin size does not necessarily result in enhanced performance metrics, as in Table II indicated, which also holds true for the baseline itself.

V. DISCUSSION

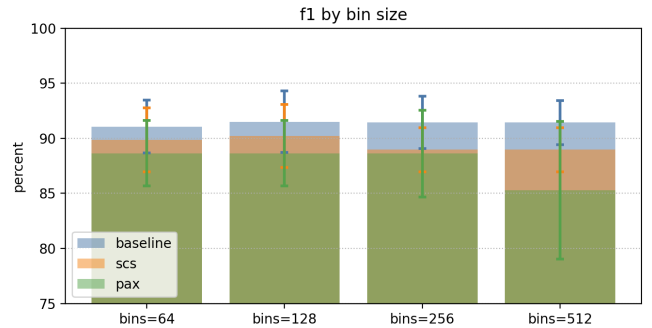
The results empirically support the convergence analysis by showing that FedSCS-XGB reaches the regime predicted by

TABLE II
CLIENT-WISE ACCURACY AND F1-SCORE FOR CENTRALIZED XGBOOST (BASELINE), FEDSCS-XGB (SCS), AND PAX ACROSS HISTOGRAM BIN COUNTS.

Client	Method	Histogram bins							
		64		128		256		512	
		Acc.	F1	Acc.	F1	Acc.	F1	Acc.	F1
patient01	baseline	92.66	89.86	93.01	90.10	93.28	90.90	93.10	90.39
	scs	90.83	87.34	91.18	86.70	91.44	88.54	91.44	88.54
	pax	89.26	86.14	89.26	86.14	89.35	86.24	85.59	81.56
patient02	baseline	94.34	91.46	93.93	90.68	94.43	91.33	94.18	91.22
	scs	94.51	91.45	95.25	92.17	94.34	89.81	94.34	89.81
	pax	92.71	88.71	92.71	88.71	93.03	88.98	92.30	87.97
patient03	baseline	97.31	92.87	97.02	94.00	96.73	92.83	96.92	93.29
	scs	96.64	91.96	96.73	90.98	96.92	91.73	96.92	91.73
	pax	96.35	92.20	96.35	92.20	96.92	92.93	96.06	91.00
patient04	baseline	93.59	92.95	93.77	93.13	93.59	93.01	93.59	92.83
	scs	90.74	88.50	92.64	90.99	90.82	87.90	90.82	87.90
	pax	91.17	89.87	91.17	89.87	90.13	88.59	88.14	85.84
patient05	baseline	96.97	85.63	97.24	85.40	97.61	85.97	97.70	87.14
	scs	96.23	84.19	96.78	84.89	96.23	84.95	96.23	84.95
	pax	96.88	83.09	96.88	83.09	95.13	80.50	88.05	71.75
patient06	baseline	97.11	92.52	97.48	92.49	97.02	91.48	97.48	92.45
	scs	96.65	92.17	94.97	91.02	95.15	90.11	95.15	90.11
	pax	95.06	89.98	95.06	89.98	95.25	88.60	94.97	89.45
patient07	baseline	96.51	91.99	96.51	92.83	96.42	92.91	96.42	92.90
	scs	96.06	91.43	96.51	92.08	95.61	89.92	95.61	89.92
	pax	93.37	87.67	93.37	87.67	94.62	90.54	91.49	84.97
patient08	baseline	96.22	91.28	97.00	93.45	97.09	93.10	96.51	91.22
	scs	95.74	91.78	96.61	92.92	94.86	88.77	94.86	88.77
	pax	96.42	91.45	96.42	91.45	96.22	92.54	94.77	89.74
ALL	baseline	95.59±1.79	91.07±2.42	95.75±1.84	91.51±2.81	95.77±1.72	91.44±2.38	95.74±1.83	91.43±2.01
	scs	94.67±2.49	89.85±2.90	95.08±2.11	90.22±2.86	94.42±2.19	88.97±2.00	94.42±2.19	88.97±2.00
	pax	93.90±2.76	88.64±2.97	93.90±2.76	88.64±2.97	93.83±2.78	88.62±3.95	91.42±3.82	85.28±6.26



(a) Acc.



(b) F1.

Fig. 3. Performance illustration of FedSCS, PAX and XGBoost-baseline for varying bin sizes.

the sufficient, non-constructive proof using practical hyperparameter choices. While the analysis guarantees existence of a sketch accuracy level α that ensures proximity to the centralized objective, the experiments demonstrate that this regime is attainable without excessive bin counts. Compared to PAX, the improved performance and reduced client-wise variability suggest that explicit global bin alignment is more effective than party-adaptive surrogate representations in heterogeneous federated settings. Although the evaluation is conducted on a cleanly recorded HAR dataset, these properties are particularly relevant for wearable-based monitoring of individuals with

spinal cord injury, where sensor noise, subject-specific movement patterns, and physiological variability are common. The observed robustness across clients indicates that FedSCS-XGB is well suited as extendable foundation for federated activity and vital-sign modeling under such real-world conditions. It should be noted that FedSCS-XGB does not yet support personalization.

VI. CONCLUSION

We presented FedSCS-XGB, a server-centric surrogate protocol for federated XGBoost, and showed both theoretically and empirically that it can closely approximate centralized

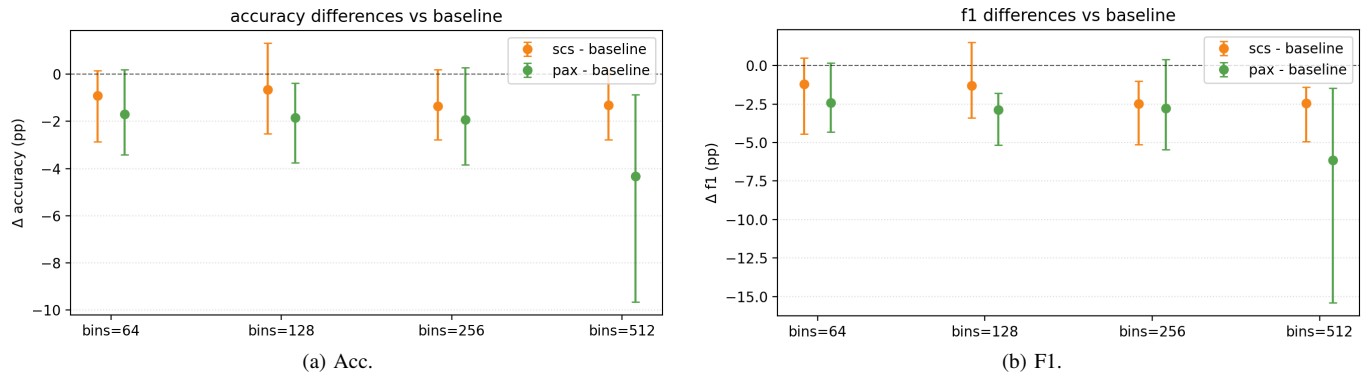


Fig. 4. Comparison of the performance gap between FedSCS and PAX to XGboost-baseline.

histogram XGBoost under sufficient hyperparameterization. Compared to PAX, FedSCS-XGB achieves higher accuracy and F1-scores with improved stability across clients. These results highlight global Hessian-weighted bin alignment as a key mechanism for effective federated tree-based learning.

Future work will extend the approach to noisy, longitudinal wearable datasets and personalized modeling of activity and physiological signals in real-world SCI cohorts.

ACKNOWLEDGMENT

This work was supported by the Federal Ministry of Research, Technology and Space (BMFTR, Germany) as part of NeuroSys: Efficient AI-methodes for neuromorphic computing in practice (Projekt D) - under Grant 03ZU2106DA. And by the Schweizer Paraplegiker Stiftung and the ETH Zürich Foundation (2021-HS-348) - Digital Transformation in Personalized Healthcare. Data used in this project were conducted in compliance with relevant Swiss laws, institutional guidelines, and the Declaration of Helsinki. The study protocol was reviewed and approved by the Ethics Committee of Northwestern and Central Switzerland, EKNZ-2023-00400 (approved on 25.04.2023).

REFERENCES

- [1] J. J. Bresnahan, B. R. Scoblionko, D. Zorn, D. E. Graves, and E. R. Viscusi, "The demographics of pain after spinal cord injury: a survey of our model system," *Spinal Cord Series and Cases*, vol. 8, no. 1, p. 14, Jan. 2022. [Online]. Available: <https://www.nature.com/articles/s41394-022-00482-1>
- [2] M. Glisic and colleagues, "Changes in secondary health conditions among individuals with spinal cord injury after transition from inpatient rehabilitation to community living," *American Journal of Physical Medicine & Rehabilitation*, vol. 103, no. 11S, p. S260, Nov. 2024.
- [3] M. Ejtehadi, S. Amrein, I. Eriks Hoogland, R. Riener, and D. Paez-Granados, "Learning Activities of Daily Living from Unobtrusive Multimodal Wearables: Towards Monitoring Outpatient Rehabilitation," in *IEEE International Conference on Rehabilitation Robotics (ICORR)*. Singapore: IEEE, 9 2023, pp. 1–7. [Online]. Available: <https://www.research-collection.ethz.ch/handle/20.500.11850/619499>
- [4] S. Bensland, A. Paul, L. Grossmann, I. Eriks-Hogland, R. Riener, and D. Paez-Granados, "Healthcare Monitoring for SCI individuals: Learning Activities of Daily Living through a SlowFast Network," in *IEEE International Conference on System Integration*, 1 2023. [Online]. Available: <https://doi.org/10.1109/SII55687.2023.10039043>
- [5] M. Elgendi, A. Yu, S. Bhutani, and C. Menon, "Balancing cardiac privacy with quality in video recordings," *Communications Medicine*, vol. 5, no. 486, 2025.
- [6] P. Vepakomma, O. Gupta, T. Swedish, and R. Raskar, "Split learning for health: Distributed deep learning without sharing raw patient data," arXiv, Tech. Rep. arXiv:1812.00564, Dec. 2018, arXiv:1812.00564 [cs, stat] type: article. [Online]. Available: <http://arxiv.org/abs/1812.00564>
- [7] S. Kalabakov, B. Jovanovski, V. Rakovic, D. Denkovski, B. Pfitzner, O. Konak, B. Arnrich, and H. Gjoreski, "Federated learning for activity recognition: A system-level perspective," *IEEE Access*, 2024.
- [8] T. Chen and C. Guestrin, "XGBoost: A scalable tree boosting system," in *Proceedings of the 22nd ACM SIGKDD International Conference on Knowledge Discovery and Data Mining*, 2016, pp. 785–794.
- [9] J. Friedman, "Greedy Function Approximation: A Gradient Boosting Machine," *The Annals of Statistics*, vol. 29, Nov. 2000.
- [10] C. Molnar, *Interpretable Machine Learning*, 2019, online book, Chapter 9: Interpretable Models – Decision Trees. [Online]. Available: <https://christophm.github.io/interpretable-ml-book/>
- [11] Y. S. Ong, B. Hooi, B. Q. Ho, D. S. Z. Sng, and O. S. Y. Goh, "Adaptive histogram-based gradient boosted trees for federated learning," in *2020 IEEE International Conference on Big Data*, 2020, pp. 1171–1180.
- [12] D. J. Beutel, T. Topal, A. Mathur, X. Qiu, J. Fernandez-Marques, Y. Gao, L. Sani, K. H. Li, T. Parcollet, P. P. B. d. Gusmão, and N. D. Lane, "Flower: A Friendly Federated Learning Research Framework," Mar. 2022, arXiv:2007.14390 [cs]. [Online]. Available: <http://arxiv.org/abs/2007.14390>
- [13] O. Aouedi, A. Sacco, L. U. Khan, D. C. Nguyen, and M. Guizani, "Federated learning for human activity recognition: Overview, advances, and challenges," *IEEE Open Journal of the Communications Society*, vol. 5, pp. 7341–7367, 2024.
- [14] K. Sozinov, V. Vlassov, and S. Girdzijauskas, "Human activity recognition using federated learning," in *IEEE Intl Conf on Parallel & Distributed Processing with Applications (ISPA)*, 2018, pp. 1103–1111.
- [15] F. Concone, C. Ferdico, G. L. Re, and M. Morana, "A federated learning approach for distributed human activity recognition," in *IEEE Int. Conf. on Smart Computing (SMARTCOMP)*, 2022, pp. 269–274.
- [16] X. Zhou, W. Liang, J. Ma, Z. Yan, and K. I.-K. Wang, "2d federated learning for personalized human activity recognition in cyber-physical-social systems," *IEEE Internet of Things Journal*, 2022.
- [17] X. Ouyang, Z. Xie, J. Zhou, G. Xing, and J. Huang, "Clusterfl: A clustering-based federated learning system for human activity recognition," *ACM Transactions on Sensor Networks*, vol. 19, no. 1, pp. 1–32, 2023.
- [18] Y. Chen, C. Yu, X. Qin, W. Gao, and J. Wang, "Fedhealth: A federated transfer learning framework for wearable healthcare," *IEEE Intelligent Systems*, 2020.
- [19] D. Cheng, L. Zhang, X. Wang, H. Wu, and A. Song, "Protohar: Prototype-guided personalized federated learning for human activity recognition," *IEEE Transactions on Neural Networks and Learning Systems*, 2023.
- [20] C. Li, D. Niu, B. Jiang, X. Zuo, and J. Yang, "Meta-har: Federated representation learning for human activity recognition," in *Proceedings of the Web Conference (WWW)*, 2021, pp. 912–922.

- [21] P. Wang, T. Ouyang, Q. Wu, Q. Huang, J. Gong, and X. Chen, "Hydra: Hybrid-model federated learning for human activity recognition on heterogeneous devices," *Journal of Systems Architecture*, vol. 147, p. 103052, 2024.
- [22] L. Tu, X. Ouyang, J. Zhou, Y. He, and G. Xing, "Feddl: Federated learning via dynamic layer sharing for human activity recognition," in *Proc. 19th ACM Conference on Embedded Networked Sensor Systems (SenSys)*, 2021, pp. 15–28.
- [23] R. Gajanin, A. Danilenka, A. Morichetta, and S. Nastic, "Towards adaptive asynchronous federated learning for human activity recognition," in *Proc. 14th Int. Conf. on the Internet of Things*, 2024.
- [24] Z. Xiao, X. Xu, H. Xing, F. Song, X. Wang, and B. Zhao, "A federated learning system with enhanced feature extraction for human activity recognition," *Knowledge-Based Systems*, vol. 229, p. 107338, 2021.
- [25] K. Jones, Y. J. Ong, Y. Zhou, and N. Baracaldo, "Federated XGBoost on Sample-Wise Non-IID Data," Sep. 2022, arXiv:2209.01340 [cs]. [Online]. Available: <http://arxiv.org/abs/2209.01340>
- [26] C. Ma, X. Qiu, D. J. Beutel, and N. D. Lane, "Gradient-less Federated Gradient Boosting Trees with Learnable Learning Rates," in *Proceedings of the 3rd Workshop on Machine Learning and Systems*, May 2023, pp. 56–63, arXiv:2304.07537 [cs]. [Online]. Available: <http://arxiv.org/abs/2304.07537>
- [27] W. Lindskog, C. Prehofer, and S. Singh, "Histogram-Based Federated XGBoost using Minimal Variance Sampling for Federated Tabular Data," in *2023 Eighth International Conference on Fog and Mobile Edge Computing (FMEC)*, Sep. 2023, pp. 182–189, arXiv:2405.02067 [cs]. [Online]. Available: <http://arxiv.org/abs/2405.02067>
- [28] M. Bodynek, F. Leiser, S. Thiebes, and A. Sunyaev, "Applying Random Forests in Federated Learning: A Synthesis of Aggregation Techniques," in *Wirtschaftsinformatik 2023 Proceedings*, 2023. [Online]. Available: <https://publikationen.bibliothek.kit.edu/1000162020>
- [29] M. Ejtehadi, G. E. Graham, C. Ringstrom, E. Du, R. Riener, and D. Paez-Granados, "Tifex-py: Time-series feature extraction for python in a human activity recognition scenario," in *2025 International Conference On Rehabilitation Robotics (ICORR)*, 2025, pp. 1332–1339.
- [30] Y. J. Ong, Y. Zhou, N. Baracaldo, and H. Ludwig, "Adaptive Histogram-Based Gradient Boosted Trees for Federated Learning," Dec. 2020, arXiv:2012.06670 [cs]. [Online]. Available: <http://arxiv.org/abs/2012.06670>
- [31] J. Masson *et al.*, "Ddskech: A fast and fully-mergeable quantile sketch with relative-error guarantees," *Proceedings of the VLDB Endowment*, vol. 12, no. 12, pp. 2190–2201, 2019.